Neurobiology of Aging 34 (2013) 1644–1652

Contents lists available at SciVerse ScienceDirect

Neurobiology of Aging

journal homepage: www.elsevier.com/locate/neuaging

Cortical atrophy and hypoperfusion in a transgenic mouse model of Alzheimer's disease

François Hébert [a,1], Marilyn Grand'Maison [a,1], Ming-Kai Ho [a], Jason P. Lerch [c], Edith Hamel [b], Barry J. Bedell [a,*]

[a] Small Animal Imaging Lab, McConnell Brain Imaging Centre, Montreal Neurological Institute, McGill University, 3801 University Street, Montreal, Quebec, Canada, H3A 2B4
[b] Laboratory for Cerebrovascular Physiology, Department of Neurology & Neurosurgery, Montreal Neurological Institute, McGill University, 3801 University Street, Montreal, Quebec, Canada, H3A 2B4
[c] Mouse Imaging Centre, Hospital for Sick Kids, 25 Orde Street, Toronto, Ontario, Canada, M5T 3H7

ARTICLE INFO

Article history:
Received 17 October 2012
Received in revised form 24 November 2012
Accepted 26 November 2012
Available online 27 December 2012

Keywords:
Alzheimer's disease
APP mouse model
Cerebral perfusion
Cortical thickness
Magnetic resonance imaging

ABSTRACT

Magnetic resonance imaging studies have revealed distinct patterns of cortical atrophy and hypoperfusion in patients with Alzheimer's disease. The relationship between these in vivo imaging measures and the corresponding underlying pathophysiological changes, however, remains elusive. Recently, attention has turned to neuroimaging of mouse models of Alzheimer's disease in which imaging-pathological correlations can be readily performed. In this study, anatomical and arterial spin labeling perfusion magnetic resonance imaging scans of amyloid precursor protein transgenic and age-matched wild-type mice were acquired at 3, 12, and 18 months of age. Fully-automated image processing methods were used to derive quantitative measures of cortical thickness and perfusion. These studies revealed increased regional cortical thickness in young transgenic mice relative to age-matched wild-type mice. However, the transgenic mice generally demonstrated a greater rate of cortical thinning over 15 months. Cortical perfusion was significantly reduced in young transgenic mice in comparison with wild-type mice across most brain regions. Previously unreported regional genotype differences and age-related changes in cortical thickness and cerebral perfusion were identified in amyloid precursor protein transgenic and wild-type mice.

1. Introduction

Noninvasive neuroimaging-based measures of regional cerebral perfusion, metabolism, and structure are increasingly used to improve our understanding of the natural evolution of Alzheimer's disease (AD) and to evaluate response to therapeutic intervention. [^{18}F]2-Fluoro-2-deoxyglucose (FDG) positron emission tomography (PET) has been extensively used in AD studies, and characteristic patterns of AD-associated glucose hypometabolism have emerged (Mosconi et al., 2010; Mosconi and McHugh, 2011). Given the wider availability of magnetic resonance imaging (MRI) compared with PET scanners, it is highly desirable to identify similar MRI-based measures of brain function. Strong concordance between regional hypoperfusion and glucose hypometabolism measured by arterial spin labeling (ASL) perfusion MRI and FDG PET, respectively, has recently been demonstrated in patients with AD (Chen et al., 2011b). Regional cerebral hypoperfusion has been suggested to be an early imaging biomarker for AD (Alsop et al., 2010; Chao et al., 2010), and large-scale studies using ASL MRI, such as the Alzheimer's Disease Neuroimaging Initiative (ADNI-2) (Jack et al., 2010), are currently underway. These cerebral blood flow (CBF) and metabolism measures are complemented by quantitative, structural information derived from anatomical MR images. Volume- and surface-based morphometry measures have revealed well-defined patterns of brain atrophy across the spectrum of AD progression (reviewed by Lin et al., 2012).

Recent studies have demonstrated that structural and functional brain alterations have distinct spatial patterns. Chen et al. (2011a) found that the regional effects of age on CBF, which were most prominent in the superior frontal, orbitofrontal, superior parietal, middle and inferior temporal, insular, precuneus, supramarginal, lateral occipital, and cingulate regions, differed from that of gray matter atrophy in normal aging. Tosun et al. (2010) performed a joint analysis of structural and perfusion MRI data in AD, and

* Corresponding author at: Montreal Neurological Institute, McGill University, 3801 University Street, Room NW-111, Montreal, Quebec, H3A 2B4, Canada. Tel.: +1 514 398 8804; fax: +1 514 398 6547.
E-mail address: barry.bedell@mcgill.ca (B.J. Bedell).
[1] These authors contributed equally to this work.

0197-4580/$ – see front matter © 2013 Elsevier Inc. All rights reserved.
http://dx.doi.org/10.1016/j.neurobiolaging.2012.11.022

determined that structural and physiological brain changes in AD provide complementary information. The analysis performed in this study also indicated that cortical thinning had a greater association with the variability of AD severity than the CBF measures. Based on these studies, an apparent dissociation between structural and cerebral perfusion measures in normal aging and AD exists, but the biological underpinnings of this counterintuitive imaging data remain elusive.

The routine clinical use of quantitative MRI and PET biomarkers for diagnosis, staging, and therapeutic efficacy monitoring in AD has been hampered by a relatively poor understanding of the pathophysiological processes underlying these measures. The ability to tightly link noninvasive imaging measures with microscopic and molecular processes in human subjects is challenging and often impossible to achieve. Alternatively, studies of animal models of AD allow for tight correlation of in vivo imaging and invasive and/or post-mortem data. Transgenic (Tg) murine models with targeted expression of mutant human amyloid precursor protein (APP) genes recapitulate many of the cognitive and neuropathological features of AD, and high-resolution images from the brains of these mice can be obtained with dedicated, high-field, small animal MRI systems.

Several recent studies have identified differences in whole or regional brain volumes between APP Tg and wild-type (WT) mice (Badea et al., 2010; Delatour et al., 2006; Lau et al., 2008; Maheswaran et al., 2009; Oberg et al., 2008). Cortical hypoperfusion has also been observed in mutant APP Tg mice by ASL MRI (Faure et al., 2011; Massaad et al., 2010; Poisnel et al., 2012; Weidensteiner et al., 2009). However, a detailed examination of the relationship between regional cortical surface morphometry and perfusion across the lifespan of APP Tg mice has not been performed.

This study examined the spatiotemporal pattern of altered cortical structure and blood flow over a 15-month period in a well-established mouse model of AD pathology by MRI. Noninvasive, whole brain, three-dimensional (3D) MRI acquisition and sophisticated, fully-automated image processing and analysis methods were used to interrogate the relationship between cortical thickness and perfusion in Tg and age-matched WT mice. The unique observations from this study provide a basis for further investigation of the complex interplay between macroscale (imaging) and microscale (cellular) processes in AD.

2. Materials and methods

2.1. Animals

Heterozygous Tg mice with neuronal overexpression of the Swedish ($670/671_{KM\rightarrow NL}$) and Indiana ($717_{V\rightarrow F}$) mutations of human APP driven by the platelet-derived growth factor β (PDGF-β) promoter on a C57BL/6J background (line J20) (Mucke et al., 2000; Tong et al., 2005) were used for these studies. This model has been well characterized for amyloidosis (Mucke et al., 2000), cognitive/behavioral impairments (Palop et al., 2003), and cerebrovascular dysfunction (Tong et al., 2005).

Separate cohorts of mice at three ages were evaluated in a cross-sectional study design, specifically young (age = 3.3 ± 0.2 months; n = 19 Tg [9 male, 10 female], 20 WT [10 male, 10 female]), middle-aged (age = 12.7 ± 1.3 months; n = 20 Tg [10 male, 10 female], 20 WT [10 male, 10 female]), old (age = 18.7 ± 0.5 months; n = 17 Tg [9 male, 8 female], 19 WT [9 male, 10 female]). Mice were housed using a 12-hour light/12-hour dark schedule and fed standard laboratory chow and water ad libitum. Experiments were approved by the Animal Ethics Committee of the Montreal Neurological Institute and McGill University, and were conducted in accordance with the guidelines of the Canadian Council on Animal Care.

2.2. In vivo MRI acquisition

Mice were anesthetized with an induction dose of 4%–5% sevoflurane and secured in an MRI-compatible bed. All MRI studies were performed under ~2.5%–3% sevoflurane in medical air and animals were allowed to breathe spontaneously without mechanical ventilation. Respiration rate and body temperature were continuously monitored using an MR-compatible system (Small Animal Instruments Inc, Stony Brook, NY, USA) and the temperature was maintained at 37 ± 0.2 °C throughout the study using a feedback-regulated warming system (Small Animal Instruments Inc, Stony Brook, NY, USA).

All MR images were obtained from a 7T Bruker Pharmascan system (Bruker Biospin, Ettlingen, Germany) using a quadrature volume resonator (RAPID MR International, Columbus, OH, USA), with an inner diameter of 28 mm. Following the acquisition of scout images, region-of-interest (ROI)-based shimming (MAPSHIM, Bruker Biospin) was performed to increase the magnetic field homogeneity within the brain. Anatomical images were acquired using a 3D balanced steady-state free precession (b-SSFP) sequence with the following parameters: matrix size, 128 × 128 × 64; field of view, 1.8 × 1.8 × 0.9 cm; spatial resolution, 140 × 140 × 140 μm; number of phase cycles, 4; and number of averages, 4. The phase-cycled images were combined using the sum-of-squares reconstruction method to minimize banding artifacts (Bangerter et al., 2004). Perfusion images were acquired with a customized, 3D pseudocontinuous ASL sequence using the following parameters: matrix size, 64 × 64 × 32; field of view, 1.8 × 1.8 × 0.9 cm; spatial resolution, 280 × 280 × 280 μm; and 48 averages. Perfusion labeling was achieved by positioning a 2-mm thick inversion slab in the neck region (~7 mm inferior to the level of the brainstem) and inverting inflowing blood within this slab every 14 milliseconds using spatially-selective sinc radiofrequency pulses. The entire scanning session lasted approximately 2.5 hours per animal.

2.3. MRI processing

An unbiased, symmetric, customized template was generated from anatomical scans from the 115 mice using an iterative process (Fonov et al., 2011; Lau et al., 2008). Before template generation, each reconstructed image volume underwent image nonuniformity correction using the N3 algorithm (Sled et al., 1998), brain masking, and linear spatial normalization using a 12-parameter affine transformation (Collins et al., 1994) to map individual images from native coordinate space to reference space. Briefly, the template generation process involved an iterative (coarse-to-fine resolution) estimation of the nonlinear transformation to match each MRI scan to the evolving average of the population. The final anatomical template (population average) was generated with an isotropic voxel resolution of 0.06 mm (Fig. 1A). This customized template was parcellated into an atlas (Fig. 1B) consisting of 14 cerebral cortical regions per hemisphere, specifically anterior cingulate cortex, auditory cortex, barrel cortex, entorhinal cortex, frontal cortex, insula, motor cortex, perirhinal cortex, piriform cortex, posterior cingulate cortex, retrosplenial cortex, somatosensory cortex 1, somatosensory cortex 2, and visual cortex, using the Montreal Neurological Institute (MNI) McConnell Brain Imaging Centre DISPLAY software package (http://www.bic.mni.mcgill.ca). The masks for the 14 cerebral cortical regions were projected onto a standardized cortical surface template for surface-based ROI analysis (Fig. 2).

For cortical thickness measurements, the cortical mask with inside, outside, interhemispheric, and resistive boundaries (Fig. 1B) was nonlinearly registered from the atlas to each subject. Streamlines running from the inner to outer boundaries of the cortex were

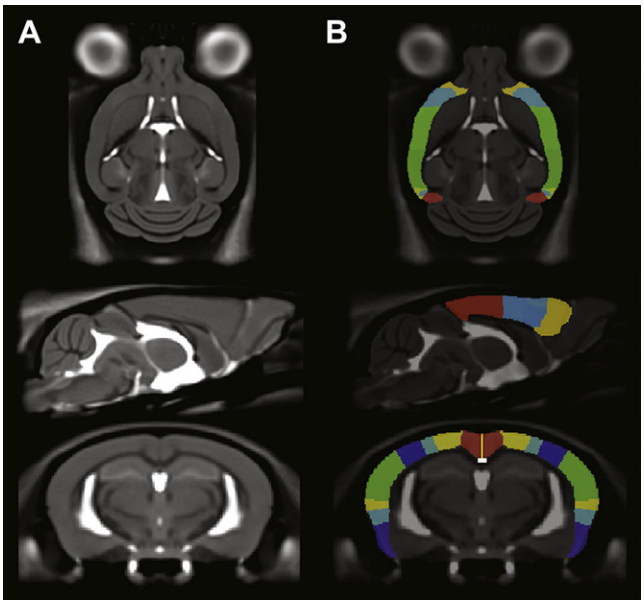

Fig. 1. Orthogonal views (axial, sagittal, and coronal, top to bottom, respectively) of the anatomical template (A) and the parcellated cortical atlas (B). Note the interhemispheric boundary (yellow line) and resistive boundary (white line) used for cortical thickness measurements in (B). The anatomical template was derived from all 115 available scans and the atlas included 14 cortical regions.

defined using Laplace's equation and their length was used as the measure of cortical thickness (Lerch et al., 2008). The mean cortical thickness was computed from an intermediate surface for each of the 14 predefined ROIs from the spatially normalized thickness maps.

The control perfusion images were linearly registered to the anatomical images for each mouse to compensate for potential slight movement during the scanning session. Parametric perfusion maps based on the fractional ASL signal, defined as the ratio between the difference [control − labeled] and control images (Borogovac and Asllani, 2012; Lu et al., 2010), were calculated on a voxel-by-voxel basis. The perfusion maps were spatially normalized to reference space using the transformations derived from the anatomical image registration. To directly compare cortical thickness and perfusion measures, the perfusion data was projected to the cortical surface by averaging the image intensity along each streamline passing through each vertex. The individual, spatially normalized perfusion maps were averaged to produce group mean parametric maps. ROI-based perfusion measures were derived using the surface MRI atlas in reference space.

2.4. Statistical analysis

Statistical analysis was performed using Matlab (Mathworks, Natick, MA, USA) and the SurfStat toolbox (http://www.math.mcgill.ca/keith/surfstat) (Worsley et al., 2009). Linear mixed-effects models using the restricted maximum likelihood (REML) estimation method were used to assess group differences and cross-sectional changes (Pinheiro and Bates, 2000). Specifically, a one-way analysis of variance (ANOVA) was used to assess between-group differences (Tg vs. WT) at each age level (young, middle-aged, old). For each genotype, a one-way ANOVA was also used to assess across-age (within-groups, cross-sectional) differences. A two-way ANOVA was used to assess the genotype-by-age interaction. Quantitative results of the vertexwise analysis are expressed as statistical parametric maps resulting from post hoc Student's two-tailed t-tests. The statistical parametric maps are presented without thresholding to demonstrate the overall pattern of group differences. For the ROI-based analysis, measures from the left and right hemispheres were combined to maximize statistical power, and quantitative results are expressed as mean ± standard deviation of the effect of interest (between-groups and cross-sectional within-groups differences). The ROI-based data was adjusted for multiple comparisons using the Bonferroni correction.

3. Results

3.1. APP Tg and WT mice exhibit age-related differences in regional cortical thickness

A globally increased mean cortical thickness was identified in the young Tg mice compared with young WT mice (Fig. 3). The ROI-based analysis (Fig. 3) demonstrated that the difference in cortical thickness (Tg > WT) in the young Tg mice was significant ($p < 0.05$) in all regions examined, except for the barrel cortex, motor cortex, and somatosensory cortex 1, which did not survive correction for multiple comparisons. This difference was greatest in the perirhinal cortex ($t = 6.2$, $p < 0.001$), posterior cingulate cortex ($t = 5.1$, $p < 0.001$), insula ($t = 4.9$, $p < 0.001$), and entorhinal cortex ($t = 4.4$, $p < 0.001$). The vertexwise t-statistic maps (Fig. 4) revealed the

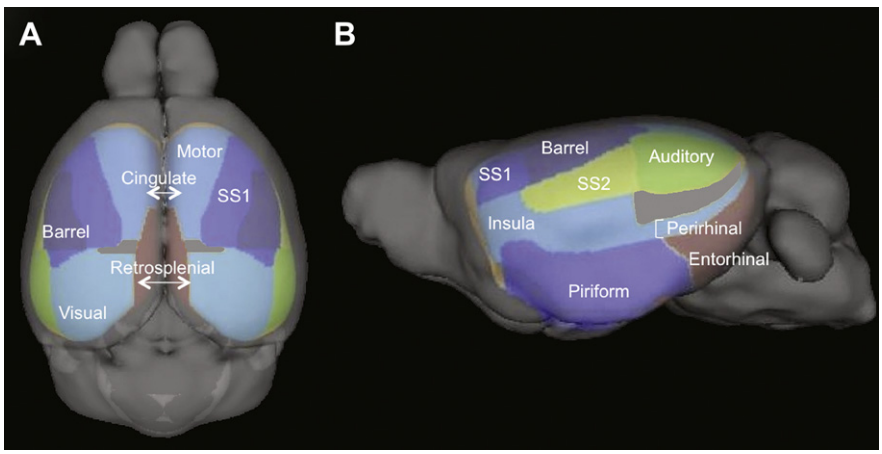

Fig. 2. Superior (A) and lateral (B) views of the cortical surface atlas with 14 region of interest labels.

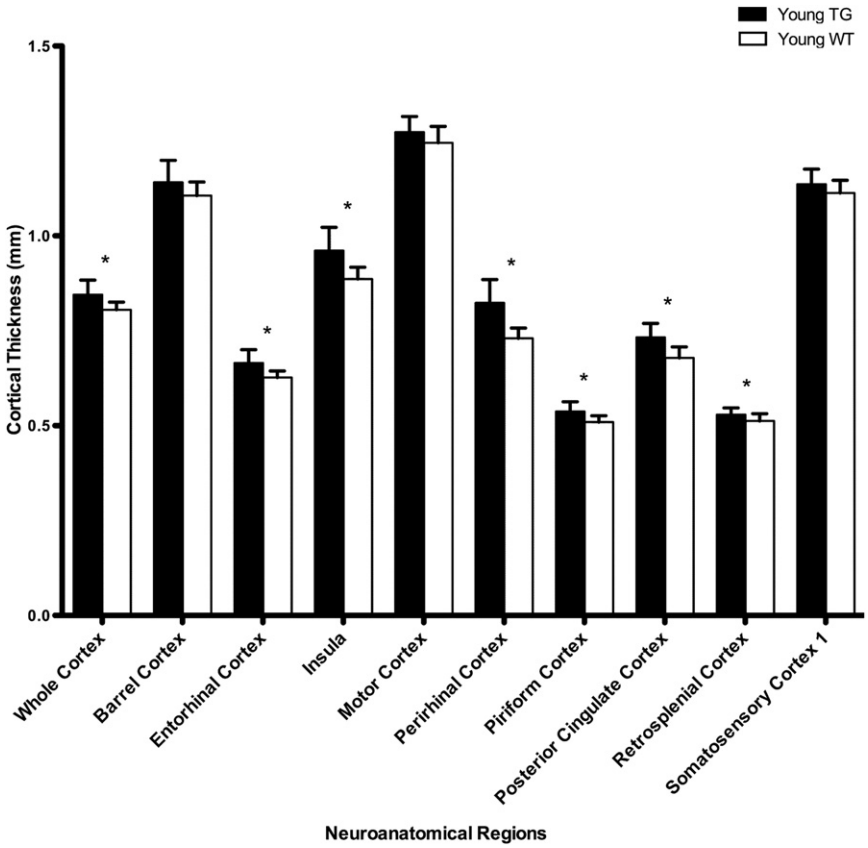

Fig. 3. Magnetic resonance imaging cortical thickness measurements from representative regions-of-interest (ROIs) in young transgenic and wild-type mouse groups. Note that the whole cortex and most regions demonstrated a greater cortical thickness in transgenic mice compared with age-matched, wild-type mice. For the sake of clarity, not all ROIs have been included. The following behavior was seen in the remaining ROIs: the anterior cingulate cortex was similar to the posterior cingulate cortex; auditory and visual cortices were similar to the motor cortex; somatosensory cortex 2 was similar to somatosensory cortex 1; and the frontal cortex was similar to the entorhinal cortex. $^{*}p < 0.05$.

spatial heterogeneity of cortical thickness differences between young Tg and WT mice.

The Tg mice showed greater thinning across the entire cortex over 15 months than the WT mice (Fig. 5A). For both Tg and WT groups, minimal change in cortical thickness was observed over the 15-month timeframe in the anterior/posterior cingulate and retrosplenial cortical regions (Figs. 6 and 7A). The remaining cortical regions demonstrated cortical thinning in both groups with greater

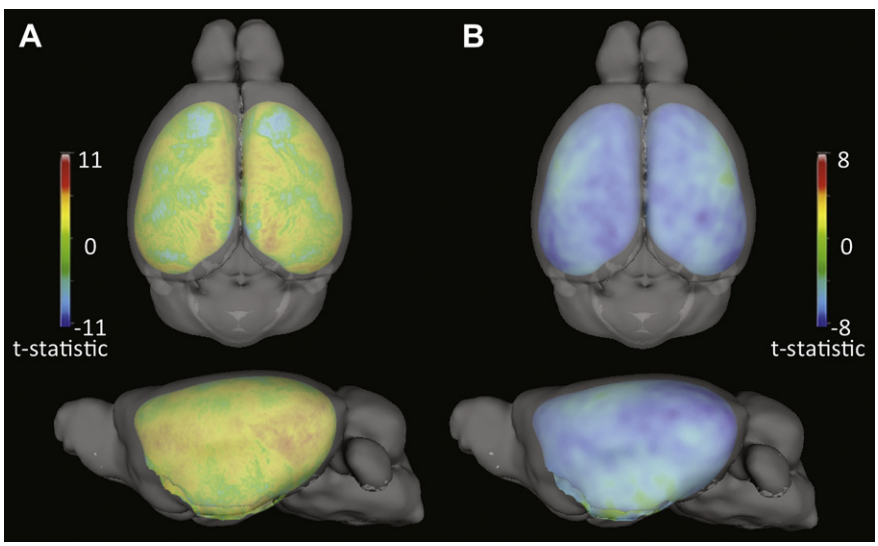

Fig. 4. Genotype group differences (transgenic vs. wild-type) in cortical thickness (A) and perfusion (B) in young (~3 months old) mice. These *t*-statistic maps demonstrate that the young transgenic mice have increased regional cortical thickness (positive values) and decreased cerebral perfusion (negative values) relative to wild-type mice before β-amyloid deposition. Note the relative symmetry in the cortical thickness and perfusion data between the left and right hemispheres. Although these maps suggest a potential negative association between loco-regional thickness and perfusion data, a significant relationship was not found.

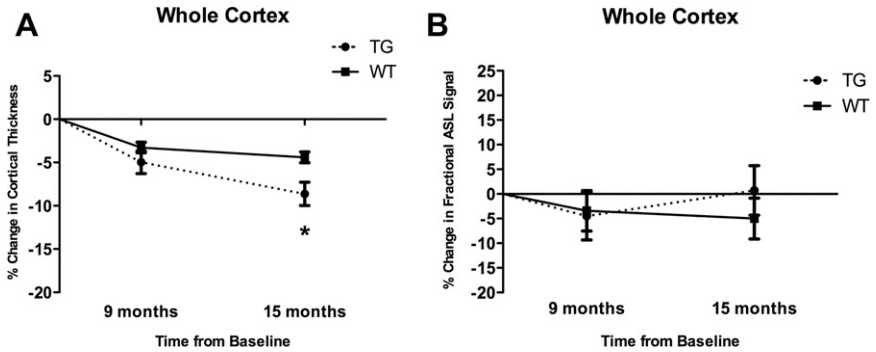

Fig. 5. Cortical thickness (A) and cortical perfusion (B) change (% change relative to young mouse group) of whole cortex over 15 months in transgenic and wild-type mice. The whole cortex showed an increased cortical thinning rate in transgenic mice relative to wild-type mice, which was statistically significant over 15 months. There was no significant difference in the rate of whole cortex perfusion change across genotypes. $^{*}p < 0.05$.

reduction in cortical thickness (i.e., atrophy) in the Tg mice relative to WT mice (Figs. 6 and 7A). Although most of these regions demonstrated significant differences in the age-by-genotype interaction at 15 months without Bonferroni correction (entorhinal cortex, $p_{\text{uncorrected}} = 0.004$; perirhinal cortex, $p_{\text{uncorrected}} = 0.016$; motor cortex, $p_{\text{uncorrected}} = 0.008$; piriform cortex, $p_{\text{uncorrected}} = 0.024$), the significance did not survive multiple comparisons. The Tg group had a higher variability than

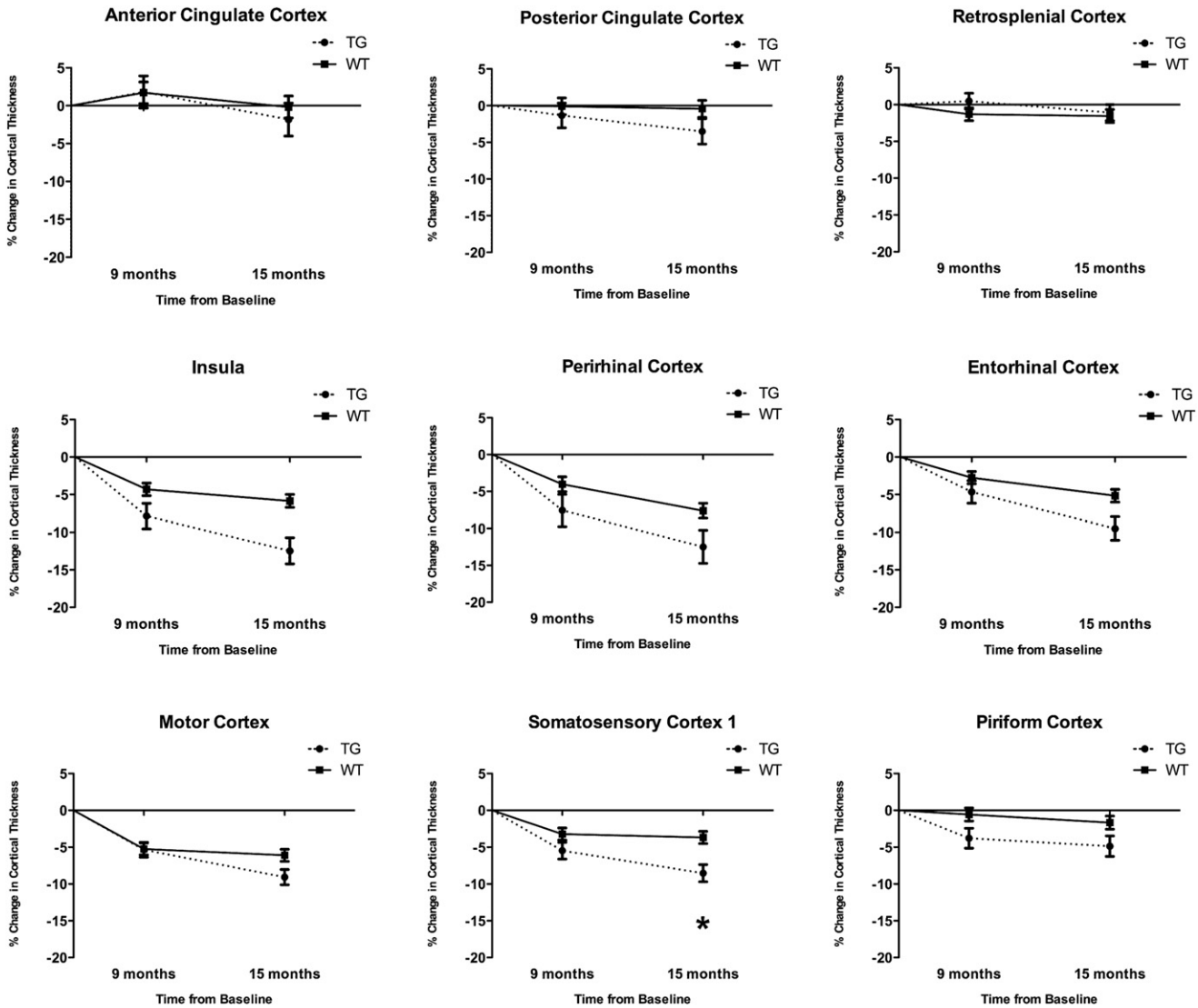

Fig. 6. Cortical thickness change (% change relative to young mouse group) over 15 months in transgenic and wild-type mice. The anterior/posterior cingulate and retrosplenial cortical regions did not show appreciable change over time. In contrast, a greater rate of cortical thinning was seen in transgenic mice than in age-matched wild-type mice in the remaining regions. For the sake of clarity, not all regions-of-interest (ROIs) have been included. The following behavior was seen in the remaining ROIs: auditory, barrel, and somatosensory 2 cortices were similar to somatosensory cortex 1; the visual cortex was similar to the motor cortex; and the frontal cortex was similar to the entorhinal cortex. $^{*}p < 0.05$.

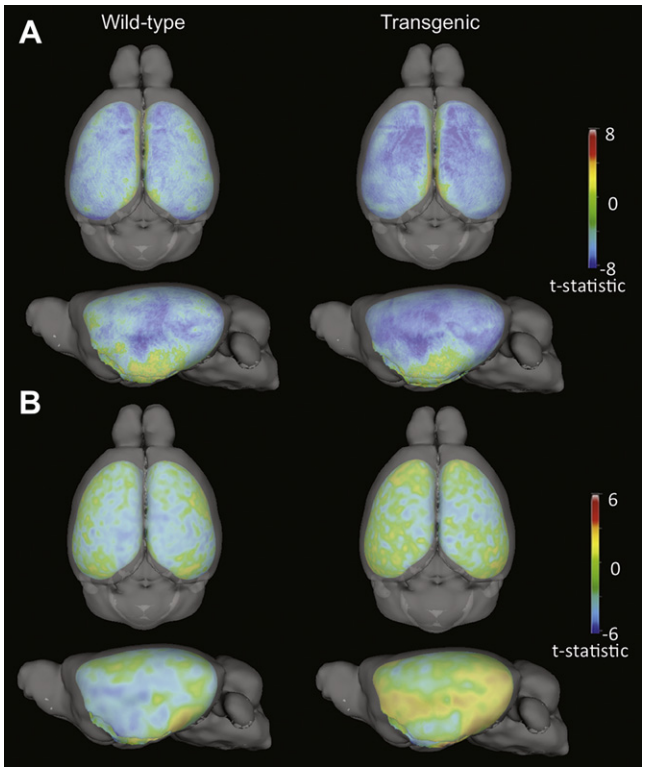

Fig. 7. Changes in cortical thickness (A) and perfusion (B) between young (~3 months old) and old (~18 months old) mice. These *t* statistic maps demonstrate that transgenic mice underwent a greater rate of local cortical thinning (negative values) relative to wild-type mice over a 15-month period (A). The maps of change in cortical perfusion (B) reveal increasing blood flow (positive values) along the rhinal fissure, including the insular, perirhinal, and entorhinal cortices, in the transgenic mice, whereas decreasing perfusion (negative values) in these regions was apparent in the wild-type mice.

the WT group likely resulting from the heterogeneity of disease progression in this model.

3.2. Tg mice demonstrate profound regional cortical hypoperfusion and distinct spatiotemporal patterns relative to WT mice

The young Tg mice demonstrated statistically significant ($p < 0.05$) hypoperfusion in all cortical regions (Figs. 4B and 8). The most significant differences were observed in perirhinal cortex ($t = 6.8$, $p < 0.001$), retrosplenial cortex ($t = 6.0$, $p < 0.001$), entorhinal cortex ($t = 5.8$, $p < 0.001$), and posterior cingulate cortex ($t = 5.7$, $p < 0.001$), which are the same regions that had the greatest differences in cortical thickness. All cortical regions remained significantly hypoperfused in the middle-aged and old Tg mice relative to the age-matched WT mice.

The change in cortical perfusion over 15 months across the whole cortex did not demonstrate a significant difference between genotypes (Fig. 5B). However, analysis of the vertexwise and regional changes revealed striking differences between Tg and WT mice (Figs. 7B and 9), indicating the importance of examining loco-regional changes, which are often obscured in global measures. The regions along the rhinal fissure, including insula ($p_{\text{uncorrected}} = 0.007$), perirhinal cortex ($p_{\text{uncorrected}} = 0.004$), and entorhinal cortex ($p_{\text{uncorrected}} = 0.036$), displayed an increasing level of perfusion over 15 months in the Tg mice, whereas stable or decreasing perfusion was observed in the WT mice. While these regions demonstrated significant differences before Bonferroni correction, this significance did not survive multiple comparisons. Although significant group differences were not identified in the other ROIs, regional heterogeneity was readily apparent.

4. Discussion

This study examined the spatiotemporal patterns of cortical thickness and resting perfusion derived from in vivo MRI scans of APP Tg and age-matched WT mice and represents the first demonstration of the regional effects of APP overexpression on both cortical structure and cerebrovascular physiology across the mouse lifespan derived from noninvasive MRI data. A striking feature of our data is the spatial and temporal heterogeneity of morphometric and functional alterations. Regional differences in cortical thickness and CBF are well documented in human MRI studies of patients with AD (Chen et al., 2011a; Lerch et al., 2005; Tosun et al., 2010), which motivated our approach to explore pathological alterations in mouse brain using fully-automated processing with vertexwise and ROI-based analysis.

The observation of increased cortical thickness in the young Tg mice was unexpected and seemingly counterintuitive. However, several studies support potential mechanisms for this finding. Plaschke et al. (1997) demonstrated that long-term cerebral hypoperfusion resulted in increased regional concentrations of APP in a rat model. Oh et al. (2009) demonstrated that overexpression of mutant (APP_{swe}) or WT APP in Tg mice can induce hypertrophy of cortical neurons. Iacono et al. (2009) identified hypertrophic cortical neurons in human autopsy material from the Nun Study and postulated that neuronal hypertrophy may constitute an early cellular response to AD pathology and/or reflect compensatory mechanisms that prevent cognitive impairment despite substantial AD-associated pathological changes. Astrogliosis is also prominent in AD and has been associated with a specific cortical laminar pattern (Beach et al., 1989). Hence, APP β-amyloid–driven neuronal hypertrophy and/or astrogliosis could potentially explain the apparent increase in cortical thickness in Tg mice. Future studies could assess cortical structure in even younger (e.g., 1 month-old) mice to investigate the age-of-onset of these pathological processes.

The regions along the interhemispheric and rhinal fissures demonstrated the most significant differences in cortical thickness between young Tg and WT mice. These areas are associated with limbic, memory, and human default-mode network–type functions, which are affected in AD. It is possible that the high constitutive activity of these regions may result in early pathological changes (Bero et al., 2011; Buckner et al., 2009). Although all of these spatially remote regions demonstrated increased thickness in young Tg mice, the regions along the interhemispheric fissure did not seem to atrophy appreciably over time, whereas the areas along the rhinal fissure displayed the greatest rate of cortical thinning. It is possible that the midline regions are more resilient than other brain regions (Driscoll and Troncoso, 2011).

Our cortical perfusion data also demonstrated heterogeneous spatial and temporal patterns. Most areas of the brain were hypoperfused in the young Tg mice. Our data from in vivo ASL MRI is consistent with the observations of Niwa et al. (2002) who identified reduced CBF in young (2–3 months old) APP Tg 2123 and 2576 mice by quantitative autoradiography. Given that mice in the Niwa study and our study do not yet exhibit amyloid plaques, soluble β-amyloid may be responsible for altered blood flow. Han et al. (2008) used digital video microscopy to demonstrate that soluble β-amyloid is a major contributor to age-dependent cerebrovascular dysfunction in Tg2576 mice. BACE1 or γ-secretase inhibitors could be used in future studies to support the role of soluble β-amyloid in the perfusion deficits observed in the young mice (without plaques and cerebral amyloid angiopathy) in our study.

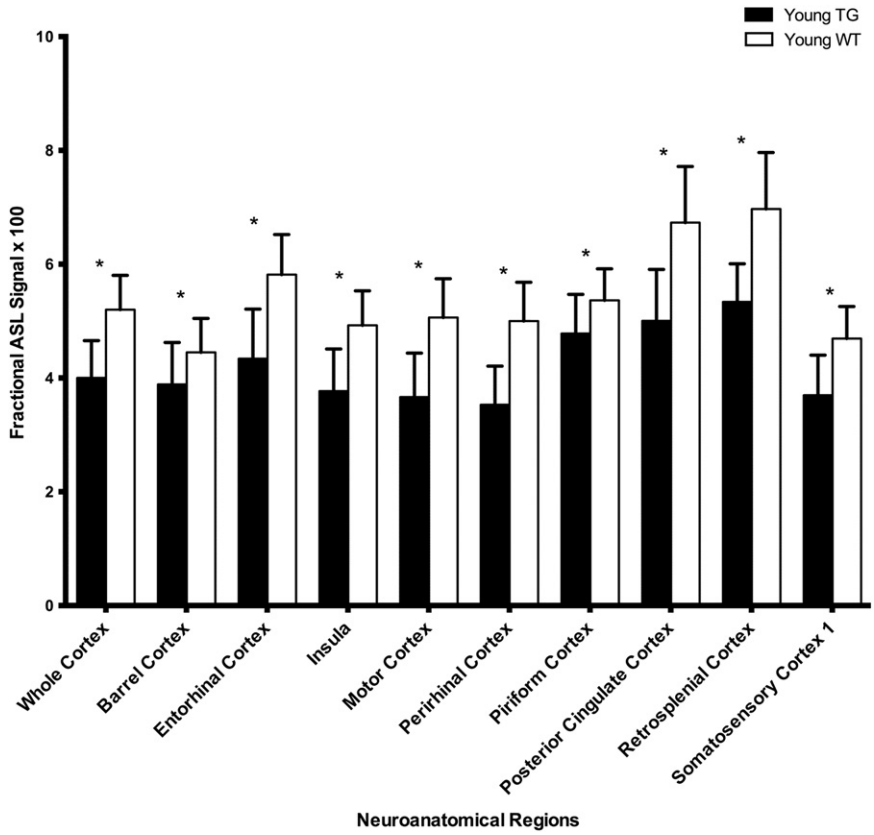

Fig. 8. Arterial spin labeling perfusion magnetic resonance imaging measurements from representative regions-of-interest (ROIs) in young transgenic and wild-type mice. Note that the whole cortex and most regions demonstrated significantly lower perfusion in transgenic mice compared with age-matched, wild-type mice. For the sake of clarity, not all ROIs have been included. The following behavior was seen in the remaining ROIs: sensory regions (auditory, visual, and somatosensory 2 cortices) were similar to the motor cortex; the anterior cingulate was similar to the posterior cingulate cortex; and the frontal cortex was similar to the entorhinal cortex. $^{*}p < 0.05$.

In addition to differences in the temporal evolution of changes in cortical thickness between the regions along the interhemispheric and rhinal fissures, these two groups of structures also demonstrated distinct patterns of age-related perfusion changes. Although the anterior/posterior cingulate and retrosplenial cortical areas showed perfusion changes (decreases) similar to WT mice, the insula and perirhinal/entorhinal regions demonstrated increased perfusion over time in Tg mice. A potential mechanism that would explain this observation includes increased local vascular density resulting from long-term angiogenesis (Desai et al., 2009). Dai et al. (2009) observed increases in regional CBF in portions of the limbic system in mild cognitive impairment (MCI) and patients with AD using ASL MRI, and suggested a compensatory cellular and/or vascular process. The apparent inverse relationship between temporal changes in cortical thickness and perfusion in these regions is particularly intriguing and it warrants further investigation into the mediators of these processes. As suggested by Dai et al. (2009), brain structural and functional changes may be asynchronous during disease evolution. Thus, animal model studies should provide new insights into findings in human AD multimodality neuroimaging studies.

A potential confounding effect of the perfusion data in this study is the use of anesthesia during MRI scanning. Inhaled anesthetic agents are known vasodilators and increased CBF has been demonstrated in rats under isoflurane (Sicard et al., 2003). Lenz et al. (1998) demonstrated that sevoflurane produces a smaller increase in CBF than isoflurane, and Flores et al. (2008) found that sevoflurane is preferred for physiological imaging in mice. Based on the literature and our own experience, these studies were performed under sevoflurane. To date, all ASL MRI and the majority of other, non-terminal, cerebrovascular physiology studies (e.g., laser Doppler flowmetry) in mice have been performed under anesthesia and it is unknown if our observed genotype- and age-related group differences in cortical perfusion are influenced by the anesthetic agent. Although imaging of awake animals may be preferable from a physiological perspective, minimizing the effects of motion is a primary concern for these sensitive MRI scans. Although Desai et al. (2010) recently reported the feasibility of optogenetic functional MRI studies in awake mice and Mizuma et al. (2010) described PET studies in conscious mice, the use of a head post for immobilization is impractical for long-term studies and the requirements for customized surface radiofrequency coils may limit accurate assessment of subcortical structures. Our group is currently investigating noninvasive methods for head restraint that will facilitate perfusion and functional MRI studies of conscious mice.

A limitation of this study is the cross-sectional design. This particular strategy was used given that the ultimate objective of our work is correlation between temporally-matched neuroimaging and neuropathology data. Longitudinal studies, which may potentially reveal more subtle group (genotype, age) differences, are being initiated in our laboratory. This study, like most AD mouse model studies, also focused on a single mouse line. Future studies should examine other APP Tg mouse models to better assess the generalizability of our results.

Substantial insight into the pathophysiological processes driving the distinct patterns of abnormal neuroanatomical structure and cerebrovascular physiology can potentially be gained by intervention with putative disease-modifying therapeutic agents

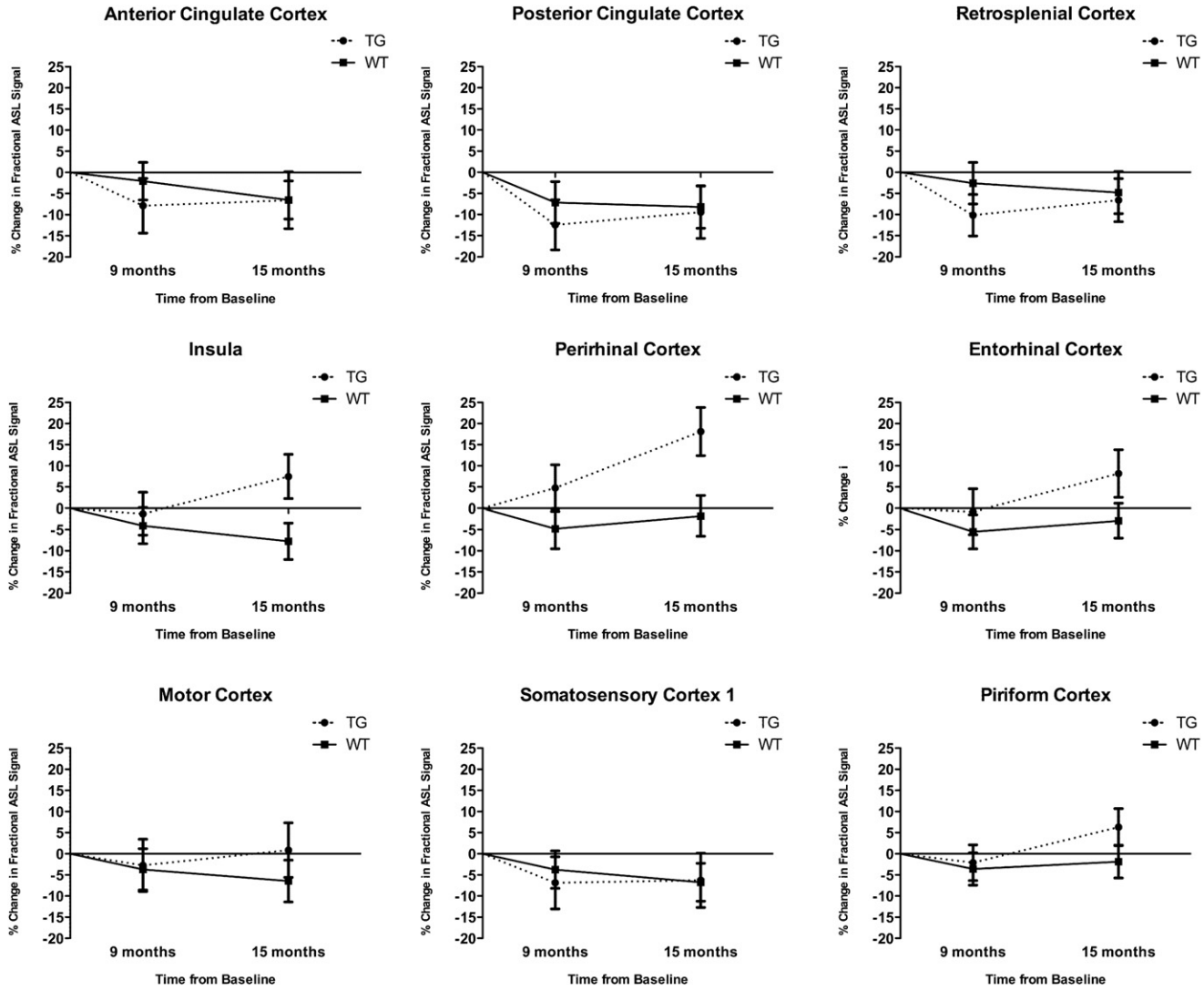

Fig. 9. Cortical perfusion change (% change relative to the young mouse group) over 15 months in transgenic and wild-type mice. The midline regions (anterior/posterior cingulate and retrosplenial cortices) and somatosensory 1 cortex showed similar decreases in perfusion over time in the transgenic and wild-type groups. In the insular, perirhinal, and entorhinal cortical regions, the transgenic mice showed increasing perfusion over time in contrast to the wild-type group. For the sake of clarity, not all regions of interest (ROIs) have been included. The following behavior was seen in the remaining ROIs: the auditory cortex was similar to the motor cortex; barrel, somatosensory 2, and visual cortices were similar to somatosensory cortex 1; and the frontal cortex was similar to the entorhinal cortex. $^{*}p < 0.05$.

with different mechanisms of action (e.g., amyloid-clearing biologics, amyloid-lowering secretase inhibitors, neuroprotective agents, neuroinflammation modulators). The noninvasive nature of 3D MRI scanning provides a distinct advantage over other techniques (e.g., autoradiography, laser Doppler flowmetry) for therapeutic studies, as it allows for longitudinal assessment of structural and physiological changes across the entire brain. Effective translation of knowledge gleaned from such preclinical imaging studies should facilitate the development of effective treatments to delay, slow, halt, and/or reverse the progression of AD.

Disclosure statement

The authors have no conflicts of interest relevant to the subject of this manuscript, including no institutional contracts relating to this research or any other agreements of the authors or their institutions that could be seen as involving a financial interest in this work.

Acknowledgements

The authors are grateful to Drs Simone Zehntner and Alex Zijdenbos (Biospective Inc, Montreal, Quebec, Canada) for their invaluable contributions to the MR image processing, and Dr Felix Carbonell (Biospective Inc, Montreal, Quebec, Canada) for assistance with the statistical analysis. The authors thank Dr Lennart Mucke and the Gladstone Institutes for use of the J20 APP mice. The authors also thank Antonio Aliaga and Kung-Yuan Lin for acquisition of the MRI data.

Funding: This work was supported by the Canadian Institutes of Health Research (Operating Grant MOP-93795 to B.J.B.).

References

Alsop, D.C., Dai, W., Grossman, M., Detre, J.A., 2010. Arterial spin labeling blood flow MRI: its role in the early characterization of Alzheimer's disease. J. Alzheimer Dis. 20, 871–880.

Badea, A., Johnson, G.A., Jankowsky, J.L., 2010. Remote sites of structural atrophy predict later amyloid formation in a mouse model of Alzheimer's disease. NeuroImage 50, 416–427.

Bangerter, N.K., Hargreaves, B.A., Vasanawala, S.S., Pauly, J.M., Gold, G.E., Nishimura, D.G., 2004. Analysis of multiple-acquisition SSFP. Magn. Reson. Med. 51, 1038–1047.

Beach, T.G., Walker, R., McGeer, E.G., 1989. Patterns of gliosis in Alzheimer's disease and aging cerebrum. Glia 2, 420–436.

Bero, A.W., Yan, P., Roh, J.H., Cirrito, J.R., Stewart, F.R., Raichle, M.E., Lee, J.M., Holtzman, D.M., 2011. Neuronal activity regulates the regional vulnerability to amyloid-β deposition. Nat. Neurosci. 14, 750–756.

Borogovac, A., Asllani, I., 2012. Arterial spin labeling (ASL) fMRI: advantages, theoretical constrains and experimental challenges in neurosciences. Int. J. Biomed. Imaging 2012, 818456. http://dx.doi.org/10.1155/2012/818456.

Buckner, R.L., Sepulcre, J., Talukdar, T., Krienen, F.M., Liu, H., Hedden, T., Andrews-Hanna, J.R., Sperling, R.A., Johnson, K.A., 2009. Cortical hubs revealed by intrinsic functional connectivity: mapping, assessment of stability, and relation to Alzheimer's disease. J. Neurosci. 29, 1860–1873.

Chao, L.L., Buckley, S.T., Kornak, J., Schuff, N., Madison, C., Yaffe, K., Miller, B.L., Kramer, J.H., Weiner, M.W., 2010. ASL perfusion MRI predicts cognitive decline and conversion from MCI to dementia. Alzheimer Dis. Assoc. Disord. 24, 19–27.

Chen, J.J., Rosas, H.D., Salat, D.H., 2011a. Age-associated reductions in cerebral blood flow are independent from regional atrophy. NeuroImage 55, 468–478.

Chen, Y., Wolk, D.A., Reddin, J.S., Korcykowski, M., Martinez, P.M., Musiek, E.S., Newberg, A.B., Julin, P., Arnold, S.E., Greenberg, J.H., Detre, J.A., 2011b. Voxel-level comparison of arterial spin-labeled perfusion MRI and FDG-PET in Alzheimer disease. Neurology 77, 1977–1995.

Collins, D.L., Neelin, P., Peters, T.M., Evans, A.C., 1994. Automatic 3D inter-subject registration of MR volumetric data in standardized Talairach Space. J. Comput. Assist. Tomogr. 18, 192–205.

Dai, W., Lopez, O.L., Carmichael, O.T., Becker, J.T., Kuller, L.H., Gach, H.M., 2009. Mild cognitive impairment and Alzheimer disease: patterns of altered cerebral blood flow at MR imaging. Radiology 250, 856–866.

Delatour, B., Guegan, M., Volk, A., Dhenain, M., 2006. In vivo and histological evaluation of brain atrophy in APP/PS1 transgenic mice. Neurobiol. Aging 27, 835–847.

Desai, B.S., Schneider, J.A., Li, J.L., Carvey, P.M., Hendy, B., 2009. Evidence of angiogenic vessels in Alzheimer's disease. J. Neural. Transm. 116, 587–597.

Desai, M., Kahn, I., Knoblich, U., Bernstein, J., Atallah, H., Yang, A., Kopell, N., Buckner, R.L., Graybiel, A.M., Moore, C.I., Boyden, E.S., 2010. Mapping brain networks in awake mice using combined optical neural control and fMRI. J. Neurophysiol. 105, 1393–1405.

Driscoll, I., Troncoso, J., 2011. Asymptomatic Alzheimer's disease: a prodrome or a state of resilience. Curr. Alzheimer. Res. 8, 330–335.

Faure, A., Verret, L., Bozon, B., El Tannir El Tayara, N., Ly, M., Kober, F., Dhenain, M., Rampon, C., Delatour, B., 2011. Impaired neurogenesis, neuronal loss, and brain function deficits in the APPxPS1-Ki mouse model of Alzheimer's disease. Neurobiol. Aging 32, 407–418.

Flores, J.E., McFarland, L.M., Vanderbilt, A., Ogasawara, A.K., Williams, S.-P., 2008. The effects of anesthetic agent and carrier gas on blood glucose and tissue uptake in mice undergoing dynamic FDG-PET imaging: sevoflurane and isoflurane compared in air and in oxygen. Mol. Imaging. Biol. 10, 192–200.

Fonov, V., Evans, A.C., Botteron, K., Almli, C.R., McKinstry, R.C., Collins, D.L., 2011. Unbiased average age-appropriate atlases for pediatric studies. NeuroImage 54, 313–327.

Han, B.H., Zhou, M.-L., Abousaleh, F., Brendza, R.P., Dietrich, H.H., Koenigsknecht-Talboo, J., Cirrito, J.R., Milner, E., Holtzman, D.M., Zipfel, G.J., 2008. Cerebrovascular dysfunction in amyloid precursor protein transgenic mice: contribution of soluble and insoluble amyloid-β peptide, partial restoration via γ-secretase inhibition. J. Neurosci. 28, 13542–13550.

Iacono, D., Markesbery, W.R., Gross, M., Pletnikova, O., Rudow, G., Zandi, P., Troncoso, J.C., 2009. The Nun Study: clinically silent AD, neuronal hypertrophy, and linguistic skills in early life. Neurology 73, 665–673.

Jack Jr., C.R., Bernstein, M.A., Borowski, B.J., Gunter, J.L., Fox, N.C., Thompson, P.M., Schuff, N., Krueger, G., Killiany, R.J., DeCarli, C.S., Dale, A.M., Weiner, M.W., the Alzheimer's Disease Neuroimaging Initiative, 2010. Update on the MRI core of the Alzheimer's Disease Neuroimaging Initiative. Alzheimers Dement. 5, 212–220.

Lau, J.C., Lerch, J.P., Sled, J.G., Henkelman, R.M., Evans, A.C., Bedell, B.J., 2008. Longitudinal neuroanatomical changes determined by deformation-based morphometry in a mouse model of Alzheimer's disease. NeuroImage 42, 19–27.

Lenz, C., Rebel, A., van Ackern, K., Kuschinsky, W., Waschke, K.F., 1998. Local cerebral blood flow, local cerebral glucose utilization, and flow-metabolism coupling during sevoflurane versus isoflurane anesthesia in rats. Anesthesiology 89, 480–488.

Lerch, J.P., Pruessner, J.C., Zijdenbos, A., Hampel, H., Teipel, S.J., Evans, A.C., 2005. Focal decline of cortical thickness in Alzheimer's disease identified by computational neuroanatomy. Cereb. Cortex 15, 995–1001.

Lerch, J.P., Carroll, J.B., Dorr, A., Spring, S., Evans, A.C., Hayden, M.R., Sled, J.G., Henkelman, R.M., 2008. Cortical thickness measured from MRI in the YAC128 mouse model of Huntington's disease. NeuroImage 41, 243–251.

Lin, A.-L., Laird, A.R., Fox, P.T., Gao, J.-H., 2012. Multimodal MRI neuroimaging biomarkers for cognitive normal adults, amnestic mild cognitive impairment, and Alzheimer's disease. Neurol. Res. Int. 2012, 907409. http://dx.doi.org/10.1155/2012/907409.

Lu, H., Leoni, R., Silva, A.C., Stein, E.A., Yang, Y., 2010. High field continuous arterial spin labeling (CASL) with long labeling duration: reduced confounds from blood transit time and post-labeling delay. Magn. Reson. Med. 64, 1557–1566.

Maheswaran, S., Barjat, H., Rueckert, D., Bate, S.T., Howlett, D.R., Tilling, L., Smart, S.C., Pohlmann, A., Richardson, J.C., Hartkens, T., Hill, D.L., Upton, N., Hajnal, J.V., James, M.F., 2009. Longitudinal regional brain volume changes quantified in normal aging and Alzheimer's APP x PS1 mice using MRI. Brain. Res. 1270, 19–32.

Massaad, C.A., Amin, S.K., Hu, L., Mei, Y., Klann, E., Pautler, R.G., 2010. Mitochondrial superoxide contributes to blood flow and axonal transport deficits in the Tg2576 mouse model of Alzheimer's disease. PLoS ONE 5, e10561. http://dx.doi.org/10.1371/journal.pone.0010561.

Mizuma, H., Shukuri, M., Hayashi, T., Watanabe, Y., Onoe, H., 2010. Establishment of in vivo brain imaging method in conscious mice. J. Nucl. Med. 51, 1068–1075.

Mosconi, L., Berti, V., Blodzik, L., Pupi, A., De Santi, S., de Leon, M.J., 2010. Pre-clinical detection of Alzheimer's disease using FDG-PET, with or without amyloid imaging. J. Alzheimer Dis. 20, 843–854.

Mosconi, L., McHugh, P.F., 2011. FDG- and amyloid-PET in Alzheimer's disease: is the whole greater than the sum of the parts? Q. J. Nucl. Mol. Imaging 55, 250–264.

Mucke, L., Masliah, E., Yu, G.Q., Mallory, M., Rockenstein, E.M., Tatsuno, G., Hu, K., Kholodenko, D., Johnson-Wood, K., McConlogue, L., 2000. High-level neuronal expression of Aβ1–42 in wild-type human amyloid protein precursor Tg mice: synaptotoxicity without plaque formation. J. Neurosci. 20, 4050–4058.

Niwa, K., Kazama, K., Younkin, S.G., Carlson, G.A., Iadecola, C., 2002. Alterations in cerebral blood flow and glucose utilization in mice overexpressing the amyloid precursor protein. Neurobiol. Dis. 9, 61–68.

Oberg, J., Spenger, C., Wang, F.-H., Andersson, A., Westman, E., Skoglund, P., Sunnemark, D., Norinder, U., Klason, T., Wahlund, L.O., Lindberg, M., 2008. Age related changes in brain metabolites observed by ^{1}H MRS in APP/PS1 mice. Neurobiol. Aging 29, 1423–1433.

Oh, E.S., Savonenko, A.V., King, J.F., Tucker, S.M.F., Rudow, G.L., Xu, G., Borchelt, D.R., Troncoso, J.C., 2009. Amyloid precursor protein increases cortical neuron size in transgenic mice. Neurobiol. Aging 30, 1238–1244.

Palop, J.J., Jones, B., Kekonius, L., Chin, J., Yu, G.Q., Raber, J., Masliah, E., Mucke, L., 2003. Neuronal depletion of calcium-dependent proteins in the dentate gyrus is tightly linked to Alzheimer's disease-related cognitive deficits. Proc. Natl. Acad. Sci. USA 100, 9572–9577.

Pinheiro, J.C., Bates, D.M., 2000. Mixed-Effects Models in S and S-PLUS. Springer, New York.

Plaschke, K., Ranneberg, T., Bauer, J., Weigand, M., Hoyer, S., Bardenheuer, H.J., 1997. The effect of stepwise cerebral hypoperfusion on energy metabolism and amyloid precursor protein (APP) in cerebral cortex and hippocampus in the adult rat. Ann. NY Acad. Sci. 826, 502–506.

Poisnel, G., Hérard, A.-S., El Tannir El Tayara, N., Bourrin, E., Volk, A., Kober, F., Delatour, B., Delzescaux, T., Debeir, T., Rooney, T., Benavides, J., Hantraye, P., Dhenain, M., 2012. Increased regional cerebral glucose uptake in an APP/PS1 model of Alzheimer's disease. Neurobiol. Aging 33, 1995–2005.

Sicard, K., Shen, Q., Brevard, M.E., Sullivan, R., Ferris, C.F., King, J.A., Duong, T.Q., 2003. Regional cerebral blood flow and BOLD responses in conscious and anesthetized rats under basal and hypercapnic conditions: implications for functional MRI studies. J. Cereb. Blood Flow Metab. 23, 472–481.

Sled, J.G., Zijdenbos, A.P., Evans, A.C., 1998. A nonparametric method for automatic correction of intensity nonuniformity in MRI data. IEEE Trans. Med. Imaging 17, 87–97.

Tong, X.-K., Nicolakakis, N., Kocharyan, A., Hamel, E., 2005. Vascular remodeling versus amyloid β-induced oxidative stress in the cerebrovascular dysfunctions associated with Alzheimer's disease. J. Neurosci. 25, 11165–11174.

Tosun, D., Mojabi, P., Weiner, M.W., Schuff, N., 2010. Joint analysis of structural and perfusion MRI for cognitive assessment and classification of Alzheimer's disease and normal aging. NeuroImage 52, 186–197.

Weidensteiner, C., Metzger, F., Bruns, A., Bohrmann, B., Kuennecke, B., von Kienlin, M., 2009. Cortical hypoperfusion in the B6.PS2APP mouse model for Alzheimer's disease: comprehensive phenotyping of vascular and tissular parameters by MRI. Magn. Reson. Med. 62, 35–45.

Worsley, K.J., Taylor, J.E., Carbonell, F., Chung, M.K., Duerden, E., Bernhardt, B., Lyttelton, O., Boucher, M., Evans, A.C., 2009. SurfStat: a Matlab toolbox for the statistical analysis of univariate and multivariate surface and volumetric data using linear mixed effects models and random field theory. Proceedings of the 15th Annual Meeting of the Organization for Human Brain Mapping, San Francisco, CA.